

# Hyperspectral core logging for fire reconstruction studies

Antonin Van Exem · Maxime Debret  · Yoann Copard · Boris Vannière  ·  
Pierre Sabatier  · Stephane Marcotte · Benoit Laignel · Jean-Louis Reys ·  
Marc Desmet

Received: 18 June 2017 / Accepted: 27 November 2017  
© Springer Science+Business Media B.V., part of Springer Nature 2017

**Abstract** Lacustrine sediments contain a wide range of proxies that enable paleoenvironmental reconstructions. For instance, charcoal can be used to document past fire regime changes. In order to analyse high-temporal- and spatial-resolution records, however, it is necessary to develop fast, low-cost and high-stratigraphic-resolution methods. We developed a new paleo-fire proxy by studying a lacustrine core from the Esterel Massif, SE France, an area affected by two recent fire events, in AD 1987 and 2003. For this purpose, we searched for charcoal deposited and preserved in the lake sediments by combining a number of complementary methods, including: classic macrocharcoal tallying, scanning spectrophotometry, scanning hyperspectral imaging and high pressure

liquid chromatography analyses. Macrocharcoal quantification is efficient, but time-consuming, and only provides intermediate-resolution data (cm scale). Spectrophotometry, used classically to quantify colour, is very fast, provides high-resolution data (4 mm) and is non-destructive (core preservation). Hyperspectral data have the same advantages as spectrophotometry, but offer higher spatial resolution (64- $\mu\text{m}$  pixel size) and higher spectral resolution (6 nm) for core logging applications. The main result of this research is based on hyperspectral analysis at very high stratigraphic resolution using the I-band index. This index usually measures reflectance values at [660, 670 nm] corresponding to the trough in red reflectance produced by Chlorophyll *a* and its diagenetic products.

---

A. Van Exem · M. Debret · Y. Copard · B. Laignel  
UNIROUEN, UNICAEN, CNRS, M2C, Normandie  
Univ., 76000 Rouen, France

B. Vannière  
Chrono-Environnement UMR 6249, MSHE USR 3124,  
CNRS, Univ. Bourgogne Franche-Comté,  
25000 Besançon, France

P. Sabatier · J.-L. Reys  
Environnement, Dynamique et Territoires de Montagne  
(EDYTEM), CNRS, University Savoie Mont Blanc,  
73373 Le Bourget du Lac, France

S. Marcotte  
INSA Rouen, UNIROUEN, CNRS, COBRA (UMR  
6014), Normandy University, avenue de l'Université,  
76800 Saint-Étienne-du-Rouvray, France

M. Desmet  
GeHCO, University of Tours, Tours, France

M. Debret (✉)  
UMR CNRS 6143 - Morphodynamique Continentale et  
Côtière, Bâtiment Blondel - UFR Sciences et Techniques,  
Université de Rouen, 76821 Mont-Saint-Aignan Cedex,  
France  
e-mail: maxime.debret@univ-rouen.fr

This [660, 670 nm] reflectance trough, however, is also affected by the presence of altered organic matter and decreases with altered organic matter such as charcoal particles. Charcoal effect on the reflectance of Chlorophyll *a* and its diagenetic products is identified on first derivative spectra by a characteristic pattern around 675 nm, which is also in agreement with the Chlorophyll *a* concentrations measured by high-pressure liquid chromatography and charcoal particles. The I-band index is hence suitable for detecting burned organic matter, by quantifying the dilution of the chlorophyll signal by the charcoal signal. Thus, this adaptation of the I-band index can be applied in fire reconstruction studies.

**Keywords** Charcoal · Fire · Paleolimnology · Lake sediments · Chlorophyll index · Hyperspectral high-resolution core logging

## Introduction

An increase in wildfires, of both their severity and area affected, is one of the expected environmental responses to global climate change (IPCC 2013). Hence, the study of long-term fire regimes and causes of change is a key aspect to assess future ecosystem responses to the projected increase in fire risk, especially in the Mediterranean area, which is subject to fire (Pausas 2004; San-Miguel-Ayanz et al. 2009; Vanni re et al. 2011, 2016). For paleofire reconstructions on centennial to millennial timescales, it is necessary to develop robust methods for the extraction of the fire signal in sediments. Fire reconstruction studies are often based on charcoal counting, which is generally carried out using pollen slide preparation or sieving methods. These are time-consuming approaches in which microcharcoal (10–150  $\mu\text{m}$ ) and macrocharcoal (usually  $> 150 \mu\text{m}$ ) particles are considered to be proxies for regional and local fires, respectively (Clark 1988; Whitlock and Millspaugh 1996; Vanni re et al. 2008). Sample preparation for this method requires chemical pre-treatment to remove carbonates, bleaching of fresh organic matter (OM) particles, and then isolation of the charcoal particles by sieving. Only thin macrocharcoal particles with well-preserved ligno-cellulosic structures and elongated shapes are counted. The occurrence of such

charcoals in sediments indicates rapid transport to the lake during and immediately after a fire episode (Vanni re et al. 2003). Stratigraphic resolution is limited by subsampling operations, while the representativeness of charcoal quantification is limited by the thickness of the sampled interval and the analysed sediment volume. These methods to reconstruct fire histories consume sediment and preclude high-resolution study (Thevenon et al. 2004; Turner et al. 2008). Therefore, there is a need to develop a method that enables (1) high-resolution analysis (2) rapid data acquisition, with (3) low analytical costs and (4) the capability to decipher the signatures of organic matter (OM) of different origins, especially recent OM and combustion residue of biomass, i.e. “black carbon material” and fossil OM.

Reflectance spectroscopy in the visible range RS-VIS appears to be a promising method. It is a rapid and non-destructive method for semi-quantitative estimation and qualitative identification of color-bearing sediment constituents (Debret et al. 2011; Trachsel et al. 2013). Spectrophotometry allows identification of the nature of the main components and qualitative changes in sediment composition (Balsam et al. 1999; Debret et al. 2006; Deaton and Balsam 1991; Balsam and Beeson 2003). In particular, spectroscopy has been proven successful in highlighting Chlorophyll *a* and its derivative products in sediments with ubiquitous troughs in the reflectance signal near 675 nm (Wolfe et al. 2006). Following a thorough investigation of the signals, Debret et al. (2011) proposed a coupling between the first derivative spectra (FDS) of the signals, the ratio between the percentage reflectance values at 700 and 400 nm and the  $L^*$  parameter (optical brightness), to indicate three OM endmembers: the altered, melanoidin-rich and Chlorophyll-rich fractions, as shown in a Q7/4 diagram.

With an aperture of 8 mm, the spectrophotometer used in this study, a Minolta 2600d, was limited to a spatial resolution of 4 mm. Thus, one challenge in the study of sediment records is to develop a method for higher-resolution sampling. In a recent development (Butz et al. 2016), a hyperspectral core scanner was tested at a sampling interval  $< 4$  mm. Here we present data from this rapid and high-resolution sampling method to track charcoal in sediments from a Mediterranean lake in the Esterel Range, France that was impacted by fires in AD 1987 and 2003. From

these studies we propose a new sedimentary proxy for fire. We compared our findings with the results from spectrophotometry, the charcoal-sieving method, liquid chromatography and well-documented historical fires.

### Study site

Lake Bresson is a reservoir that covers an area of 4700 m<sup>2</sup>. It was built in 1976 in the Esterel Massif, southeast France (Fig. 1a). The region has a Mediterranean climate characterized by high seasonality, with hot and dry summers that favour fire occurrences. The 27-ha watershed ranges from 78 to 174 m above mean sea level. Two sub-watersheds form the drainage basin, one to the north and the other to the northeast (Fig. 1a). The north-oriented watershed is drained by an ephemeral stream. The northeast-oriented sub-watershed is crossed by a path along its axis. Two ditches collect runoff water along the edge of this path. The northern slope runoff joins the ephemeral stream to the lake, whereas the southern slope runoff drains into a pond ahead of the lake. This secondary watershed is excluded from the lake's catchment area (Fig. 1b). The watershed was chosen for this study because of its geologic features, i.e. the bedrock is composed of highly crystallized volcanic rock (Rhyolithe) called Estérellite, which is devoid of fossil OM. In this catchment, the soils are poorly developed and the organic soil horizon A<sub>h</sub> is absent. Sparse litter is

produced by typical Mediterranean shrubs and overlies a mineral horizon with coarse and fine particles. Thus, sediment OM is either inherited from (1) Mediterranean shrubs in the catchment, (2) autochthonous aquatic primary productivity or (3) combustion residues caused by wildfires.

The lake is located in a fire-prone area, as shown in Fig. 1a, taken from the Inter-Ministerial Final Report on Climate Change Impact on Forest Fires (Chatry et al. 2010). The French database of fires in the Mediterranean region provides information regarding fire occurrence since 1973 (<http://www.promethee.com/>). It reveals that two fires occurred in the vicinity of the dam since it was built (Fig. 1b). The first fire started 3 km from the lake on 25 August 1987. This fire affected 2275 ha, especially to the southwest of the watershed, close to the lake. The second fire was started by accidental ignition 4 km from the lake on 25 July 2003. The fire spread over 924 ha and affected the northern parts of the watershed. The fires burned the sparse vegetation that comprises cork oak (*Quercus suber*), maritime pine trees (*Pinus pinaster*) and heather (*Erica arborea*).

Lake infilling started after the completion of the dam in 1976 via the seasonal water supply. The lake is shallow in the north and deepens toward the south to ~ 3 meters (Fig. 1c) because of the underlying topography. Two gravity cores were taken in the deepest part of the lake (43°28'4.2"N, 6°48'56.4"E). A 40-cm-long core, LR1203 (IGSN: IEM2C0018), was

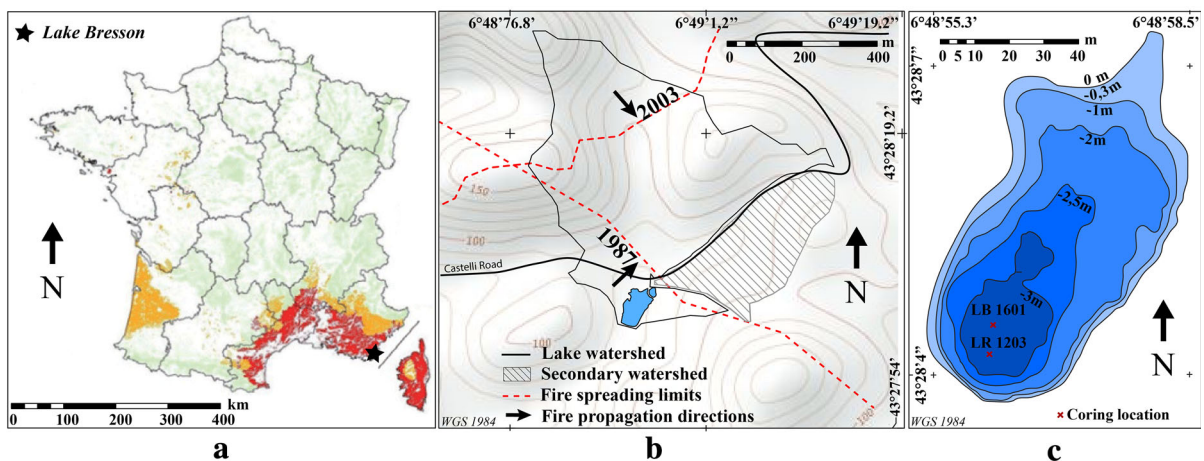


**Fig. 1** Location of Lake Bresson and past forest fires according to the “inventaire forestier national, Institut géographique national, Agence européenne de l’environnement et Météo-

France. **a** Fire-affected areas (in red and Orange). **b** Lake watershed and past fire events according to the Promethee Data base. **c** Bathymetric map and core-sampling location

sampled at a water depth of 3.55 m and a 30-cm-long core LB1601 (IGSN: IEM2C0019) was sampled at a water depth of 3.4 m. Hyperspectral imaging was used to correlate the two cores.

## Materials and methods

### Chronology

Short-lived radionuclides (gamma decay) were analyzed at 1-cm intervals using a well-type germanium detector at the Laboratoire Souterrain de Modane, following the procedure of Reyss et al. (1995). Details of the dating procedure, sedimentation rates and fluxes for this core are given in the chronology section, and throughout this paper, parentheses denote activities ( $\text{mBq g}^{-1}$ ) for  $^{210}\text{Pb}$ ,  $^{226}\text{Ra}$  and  $^{241}\text{Am}$ . Generally, counting times of 24–48 h were required to achieve a statistical error of < 10% for unsupported ( $^{210}\text{Pb}$ ) in the deepest samples and for ( $^{137}\text{Cs}$ ) peaks. In each sample from the core, the (unsupported, excess  $^{210}\text{Pb}$ ) activities were calculated by subtracting the ( $^{226}\text{Ra}$ ) activity from the total ( $^{210}\text{Pb}$ ) activity. The chronological framework was then established using these short-lived radionuclides (Goldberg 1963; Appleby and Oldfield 1992; Appleby et al. 1991) and applying the constant flux, constant sedimentation (CFCS) rate model (Goldberg 1963; Krishnaswamy et al. 1971).

### Sieving method

The presence of macrocharcoal provides evidence of fire events, but only sharp particles > 150  $\mu\text{m}$  can be considered a proxy for local fires (Vanni re et al. 2008). Accordingly, well-preserved ligno-cellulosic structured particles within the samples were counted. To remove fresh OM, hydrogen peroxide treatment was performed without mechanical action. Then, the samples were sieved using 150- $\mu\text{m}$  wire mesh before they were identified at 40  $\times$  magnification under a binocular microscope. Macrocharcoal concentration was analysed in 38 contiguous samples of approximately one cubic centimetre.

### Magnetic susceptibility

Magnetic susceptibility can be used as a proxy for terrigenous/pedogenic lithoclastic influx (Dearing

et al. 2001). The device used in this study was a Bartington “sensor” MS2E, which was moved manually. The down-core measurement interval was 4 mm, with a measurement area of 5 mm. The obtained precision was  $10^{-5}$  International System units (SI).

### Total organic carbon

Rock-Eval<sup>®</sup> pyrolysis (Vinci Technologies, France) analysis provides an estimate of total organic carbon (TOC, wt%). Based on standard analyses, uncertainties of TOC values are 0.03 wt%. Sampling was done at a resolution of 1 cm; approximately 1  $\text{cm}^3$  of sediment was sampled and dried in a ventilated oven at 25  $^\circ\text{C}$ . Subsequently, between 80 and 100 mg of dry sediment was analysed using RE6 pyrolysis. For further details of the method, see Lafargue et al. (1998).

### HPLC analysis of Chlorophyll *a*

Reversed-phase High Pressure Liquid Chromatography (HPLC) was used to determine Chlorophyll *a* concentration ( $\mu\text{g g}^{-1}$  of dry mass). Sampling was performed on core LB1601 at a resolution of 1 cm. 1 g of freeze-dried sediment was extracted with 10 mL of acetone:methanol (90:10) by sonication for 1 min in an ice bath and allowed to stand at 4  $^\circ\text{C}$  for 12 h in the dark. After centrifugation, 8 mL of the supernatant solution was filtered (PTFE, 0.22  $\mu\text{m}$ ) and evaporated to dryness under a  $\text{N}_2$  stream after addition of 100  $\mu\text{L}$  of an internal standard solution ( $\beta$ -apo-8'-carotenal 20 mg/L in acetone, Sigma Aldrich). Finally, the solution was reconstituted by addition of 1 mL acetone:water (90:10, v:v). HPLC analyses were performed on an Agilent 1100 series HPLC system (Agilent) equipped with a refrigerated autosampler (5  $^\circ\text{C}$ ), and a photo-diode array detector set at 440 and 660 nm (20 nm bandwidth). The column was a C18 Kinetex (150  $\times$  4.6, 2.6  $\mu\text{m}$ , Phenomenex, Le Peck) set at 40  $^\circ\text{C}$ . 50  $\mu\text{L}$  of the sample were mixed with 50  $\mu\text{L}$  of pyridine (0.25 M) and then injected. Eluent A was a mixture of methanol:acetone:0.25 M pyridine (50:25:25, v:v:v), adjusted to pH 6 with acetic acid. Eluent B was a mixture of methanol:acetonitrile:acetone (20:60:20, v:v:v). The mobile phase was set at 90:10 (A:B, v:v) at  $t = 0$  min and then ramped to 100% B at  $t = 35$  min (holding 5 min). The flow rate

was 1 mL/min. Calibration was performed using a standard solution of Chlorophyll *a* (DHI, Denmark).

### VIS-NIRS spectral measurements

Spectroscopic reflectance measurement describes sediment composition (Barranco et al. 1989; Balsam and Deaton 1996; Balsam et al. 1997). The device used in this study was a Konica-Minolta CM 2600d, decomposing reflected light in the visible range from 360 to 740 nm in 10-nm intervals. The illuminant was a D65 source, which corresponds to a light temperature of 6504 K, including UV. The “Excluded specular reflection” feature was used to remove mirror effects during the measurements. We performed the measurements using an 8-mm aperture every 4 mm along the core, in order to overlap the measurements. Before measuring, the thin oxidized layer was removed from the surface of the sediment and a polyethylene film was placed on the core to protect the sensor. Calibration was performed using the international white standard (BaSO<sub>4</sub>) described in Balsam et al. (1997).

Hyperspectral data were characterized by high spatial (64- $\mu$ m pixel size) and spectral resolution (6 nm), evenly distributed over a large spectral range at the University of Bern and Rouen. The camera used was a PFD-xx-V10E (Specim Ltd., Finland). Data acquisition and evaluation were done using ChemDAQ, ENVI 4.8 and IDL 8.0 software. Hyperspectral images were measured with a technical spectral resolution of 6 nm binned from 400 nm (visible domain) to 1000 nm (near-infrared domain). The spectra were measured on pixels with a spatial resolution of 64  $\mu$ m along the entire core; each pixel contains spectral information related to sediment components.

### Reflectance spectra processes

Visible spectroscopic data interpretations for sediment analyses can use the Q7/4 diagram (Debret et al. 2011, 2014) and the First derivative spectra (FDS) signatures (Barranco et al. 1989; Deaton and Balsam 1991). Here, we also used the I-band index method (Rein and Sirocko 2002).

The Q7/4 diagram plots the parameter L\* (Black/White), corresponding to the contrast indices from CIE 1976 (L\*, a\*, b\*) colour space, which is expressed as a function of the slope of the spectra on the visible

domain, determined by the ratio of the raw spectra value at 700 nm to the raw spectra value at 400 nm. The Q7/4 provides a qualitative description of sediment components and an overview of sedimentation dynamics organized between iron-rich deposits (e.g. clay), clear deposits (chalk), sediment rich in Chlorophyll *a* and its by-products, sediment rich in melanoidin-type OM and sediment rich in altered OM endmembers (Debret et al. 2011).

The FDS enables one to highlight variations on raw reflectance spectra, and specific variation patterns that characterise sediment components. FDS signatures assess OM, revealing its altered or unaltered state (Debret et al. 2011). The I-Band index was tested on the sediment from Lake Bresson because it usually gives an approximation of Chlorophyll *a* content (Rein and Sirocko 2002). The I-band index relies on absorbance by Chlorophyll *a* and its by-products in the visible domain (Schalles et al. 1998). Degradation products of chlorophyll *a* absorb at the same wavelengths in the red reflectance range [660, 670 nm] (Wolfe et al. 2006). We used the algorithm provided by Rein and Sirocko (2002), which measures the concentration by evaluating the trough in the raw reflectance spectra between 590 and 730 nm, owing to the absorbance of Chlorophyll *a* and its by-products between these wavelengths.

We used this index to assess the effect of charcoal content on the reflectance signal of Chlorophyll *a* and its by-products. Altered organic matter produced by combustion (i.e. black carbon material and charcoal) contains an aromatic ring signal (Sobkowiak et al. 1984; Guillianio et al. 1988) that interacts in the visible domain (Clark 1983; Milliken and Mustard 2007). Hence the I-band index measures the dilution of Chlorophyll *a* and its by-products signal by the charcoal signal. In this study, the I-band index may enable quantification of the interaction between the charcoal and Chlorophyll *a* signatures.

## Results

### Lithology of LR1203

The first sediment unit (U1: 40.0–37.5 cm sediment depth) is dark brown and has heterogeneous grain sizes ranging from fine clayey particles to gravel (Fig. 2). Root and twig residues were observed. The

FDS value of 0.5 at 555 nm wavelength corresponds to an Fe-oxide signature. Magnetic susceptibility is approximately  $10 \cdot 10^5$  SI units and TOC values are lower than 1.0 wt%. I-band values calculated from hyperspectral data decrease upward from 0.12 to 0.06 and from 0.11 to 0.07 for spectrophotometer data. The charcoal concentration is  $61 \text{ particles cm}^{-3}$  below 37.5 cm depth, but only one sample was measured (Fig. 2).

The second sediment unit (U2: 37.5–33.0 cm depth) is light brown and has a sharp contact with U1, expressed as a discontinuity at 37–38 cm depth. Grain sizes are homogeneous and composed of silts and clay. The FDS signature has a value of 1 at 555 nm. Magnetic susceptibility presents significant variations, from  $10 \cdot 10^5$  to  $20 \cdot 10^5$  SI units, and average TOC content is 1.0 wt%. I-band values are lower in U2: 0.05 for hyperspectral and 0.1 for spectrophotometer data. Charcoal concentrations display important variations ( $61, 108, 17, 26 \text{ particles cm}^{-3}$ ), but remain much lower than in the next sediment unit.

The third unit (U3: 33.0–26.5 cm depth) is black to dark brown and composed of clay; a black layer marks the transition from U2 (Fig. 2). The value of the FDS

at 555 nm is the lowest of the core, but its intensity remains high (approximately 0.4). Magnetic susceptibility increases strongly up to  $50 \cdot 10^5$  SI. The TOC values range from 1.50 to 1.90 wt% except for the black layer in which values reach 2.20 wt%. I-band values show a sharp peak at 33 cm and decrease all along U3. Charcoal concentrations reveal two peaks:  $139 \text{ particles cm}^{-3}$  (29.5 cm depth) and  $209 \text{ particles cm}^{-3}$  (31.5 cm depth).

The fourth unit (U4: 26.5–0.0 cm depth) is brown and composed of silty clay sediments. A black layer observed at 0.5 cm depth shows a heterogeneous grain size and is composed of silts and fine sands that contain a few plant fragments. The FDS signature of Fe-oxide at 555 nm is high and increases in intensity along the unit from 0.5 to 1. Magnetic susceptibility decreases from  $25 \cdot 10^5$  to  $10 \cdot 10^5$  SI. TOC values increase from 1.44 to 3.55 wt%. The I-band varies between 0.11 and 0.08, with a marked increase in the black layer at 0.5 cm sediment depth. Charcoal concentrations remain lower than  $50 \text{ particles cm}^{-3}$ , with the exception of the top black layer in which the concentration reaches  $118 \text{ particles cm}^{-3}$ .

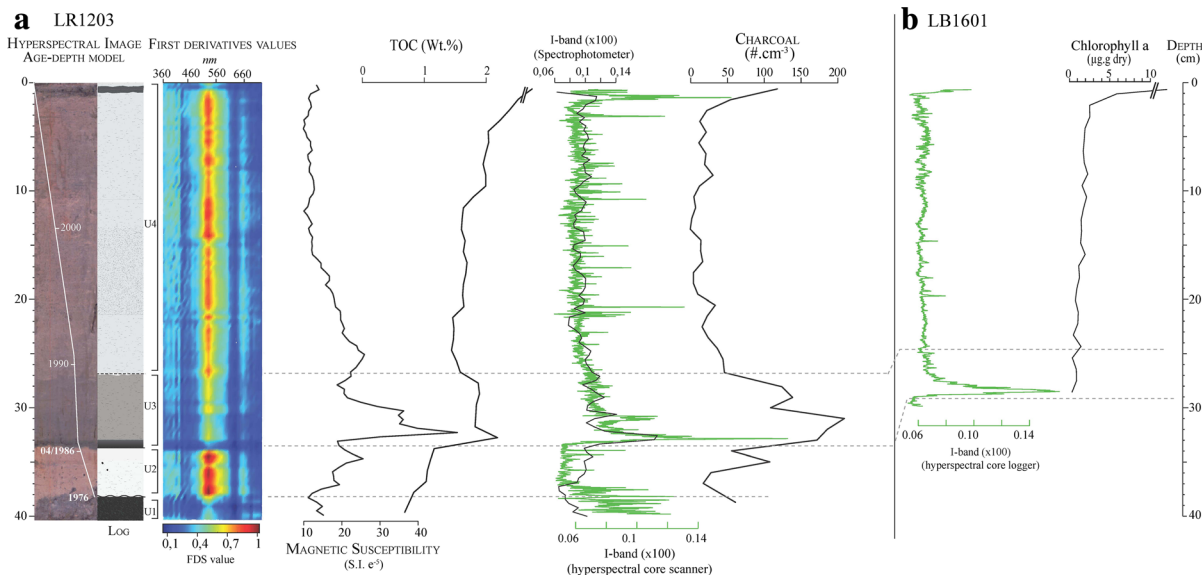


**Fig. 2** **a** Hyperspectral image, sediment log, first derivative spectra (FDS), magnetic susceptibility, total organic carbon, I-band and charcoal concentration in LR1203, **b** I-band and Chlorophyll *a* concentration in LB1601. The cores are divided into four sedimentary units (U1–4) highlighted by colour

variations, as presented by the LR1203 sedimentary description. Two black layers are visible on the image and are represented on the sediment log at the base of U3 and at 0.5 cm from the sediment interface in U4

## LB1601 correlation and Chlorophyll *a* concentrations

Core correlation enables describing the Chlorophyll *a* concentrations with respect to the lake sediment lithology. We used the I-band values from hyperspectral imaging data. Two major features are easily identifiable in both cores. A peak at 33 cm in LR1203 occurs at 29 cm in LB1601. The second stratigraphic feature is the black layer present in both cores at 0.5 cm. U2, U3 and U4 are identified in LR1203 and LB1601, but U1 is not represented in LB1601.

Pigment analysis with HPLC was performed on core LB1601. The size of U2 (< 0.5 cm) precluded sampling enough material for proper HPLC analysis. In U3, Chlorophyll *a* concentrations vary between  $0.35 \mu\text{g g}^{-1}$  and  $1.45 \mu\text{g g}^{-1}$ . U4 shows the main variation, as Chlorophyll *a* concentration increases slightly from 0.5 to  $2.5 \mu\text{g g}^{-1}$  until 2.5 cm and increases sharply to  $21.79 \mu\text{g g}^{-1}$  at the top of the core.

### Age-depth model

In U4, the ( $^{210}\text{Pb}_{\text{ex}}$ ) indicates a mean accumulation rate of  $1.05 \pm 0.15 \text{ cm year}^{-1}$ , up to  $1986 \pm 2.5 \text{ years}$  at 27.5 cm (Fig. 3a). In U3, at 29.5, 31.5 and 33.5 cm, the ( $^{210}\text{Pb}_{\text{ex}}$ ) data display

constant activity, suggesting high, almost instantaneous sedimentation over this interval. The ( $^{210}\text{Pb}_{\text{ex}}$ ) profile could indicate that the increase in ( $^{137}\text{Cs}$ ) activity between 33.5 and 29.5 cm, results from a sedimentation rate change. Under this hypothesis, however, it should be accompanied by an increase in ( $^{241}\text{Am}$ ) activity, which has the same origin, the 60 atmospheric nuclear tests in 1963. Measured ( $^{241}\text{Am}$ ) activities are very low (data not shown), about 1 Bq/kg, and no increase in activity appears between 33.5 and 29.5 cm despite large statistical errors. Therefore, we assigned the ( $^{137}\text{Cs}$ ) maximum to the Chernobyl accident in 1986, which deposited ( $^{137}\text{Cs}$ ) without ( $^{241}\text{Am}$ ). Assuming that U3 was a deposit linked to the 1987 fire event (see section below), there is good agreement between the ages derived from the ( $^{210}\text{Pb}_{\text{ex}}$ )-CFCS model and the ( $^{137}\text{Cs}$ ) peak attributed to the 1986 Chernobyl accident (Fig. 3b).

Thus, in U2, the sedimentation rate was estimated to be  $0.4 \text{ cm year}^{-1}$  between the depth of the lake formation in 1976 and that of the Chernobyl accident. Accordingly, the high initial ( $^{210}\text{Pb}_{\text{ex}}$ ) activity and the sharp ( $^{210}\text{Pb}_{\text{ex}}$ ) decrease indicate a slower sedimentation rate than in the upper part of U3. In U1, the ( $^{210}\text{Pb}_{\text{ex}}$ ) and ( $^{137}\text{Cs}$ ) data display very low activities, which probably correspond to older material at this depth, probably the soils present prior to the construction of the dam in 1976.

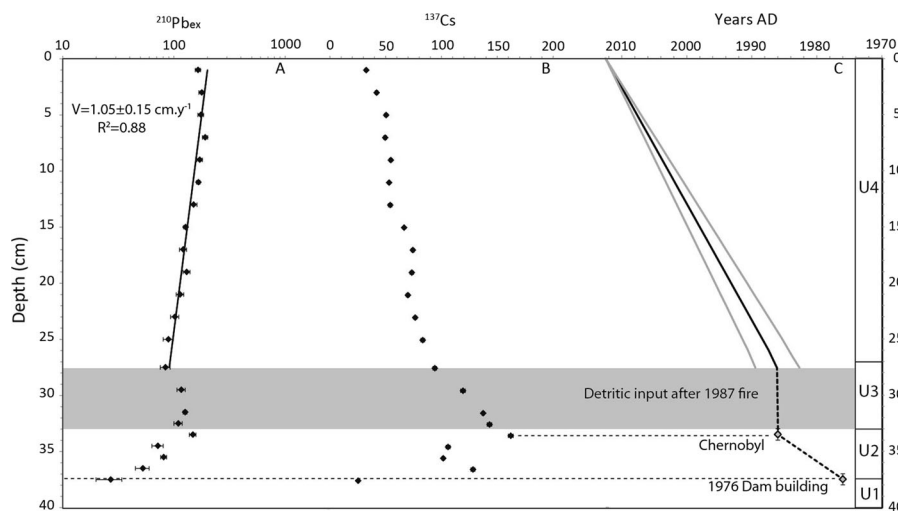


**Fig. 3** Downcore profiles of LR1203 core: (a) ( $^{210}\text{Pb}_{\text{ex}}$ ), (b) ( $^{137}\text{Cs}$ ) and (c) age model. The grey band indicates a detritic event after the 1987 fire. The right-hand part of the figure shows the sedimentary units

## Sediment composition

The Q7/4 diagram applied to the lake sediment shows a bimodal distribution, with an “Iron-rich deposit” end-member and a “Clayey deposit” end-member (Fig. 4). The FDS signals, however, reveal a hematite peak in both end-members. FDS signatures also indicate two additional OM signatures that play significant roles in identifying the sediment sources (Fig. 4). Indeed, between 590 and 730 nm, the first derivative signal is characterized by a peak at 675 nm, which highlights the well-known occurrence of Chlorophyll *a* and its diagenetic products (Wolfe et al. 2006). The second, less common OM signal has been related to carbonized OM (Debret et al. 2011). The combination of the Q7/4 diagram and FDS signals improves the sediment source fingerprinting. These methods are applied to the sedimentary units to detail the sediment composition.

U1 shows a low 700/400 ratio and an L\* value close to 40%. The FDS signals reveal the occurrence of “altered” OM, which is consistent with the numerous

counted particles of charcoal and the large amount of terrestrial plant debris, mainly roots and twigs. The heterogeneous grain sizes and discontinuous, sharp contact with the above unit, suggest that the base of the core corresponds to a buried soil on which the sediments accumulated.

U2 exhibits a major change in sediment composition, as shown by the sharp transition with the previous unit. The 700/400 ratio is somewhat higher (~ 8) and the L\* values reach 35% (Fig. 4). In the Q7/4 diagram, samples from this unit are plotted between the iron-rich deposit and the Chlorophyll *a* and diagenetic products end-members. With very homogenous fine grain sizes, this unit suggests deposition by decantation and reflects the first stage of dam filling. The first derivative signal of Chlorophyll *a* and its diagenetic products is evidence of primary productivity in the lake. The absence of a signal of altered OM is in agreement with the low concentrations of counted charcoal in the sediment core.

The transition to U3 is sharp, but without an erosion surface. The Q7/4 ratio shows intermediate values and

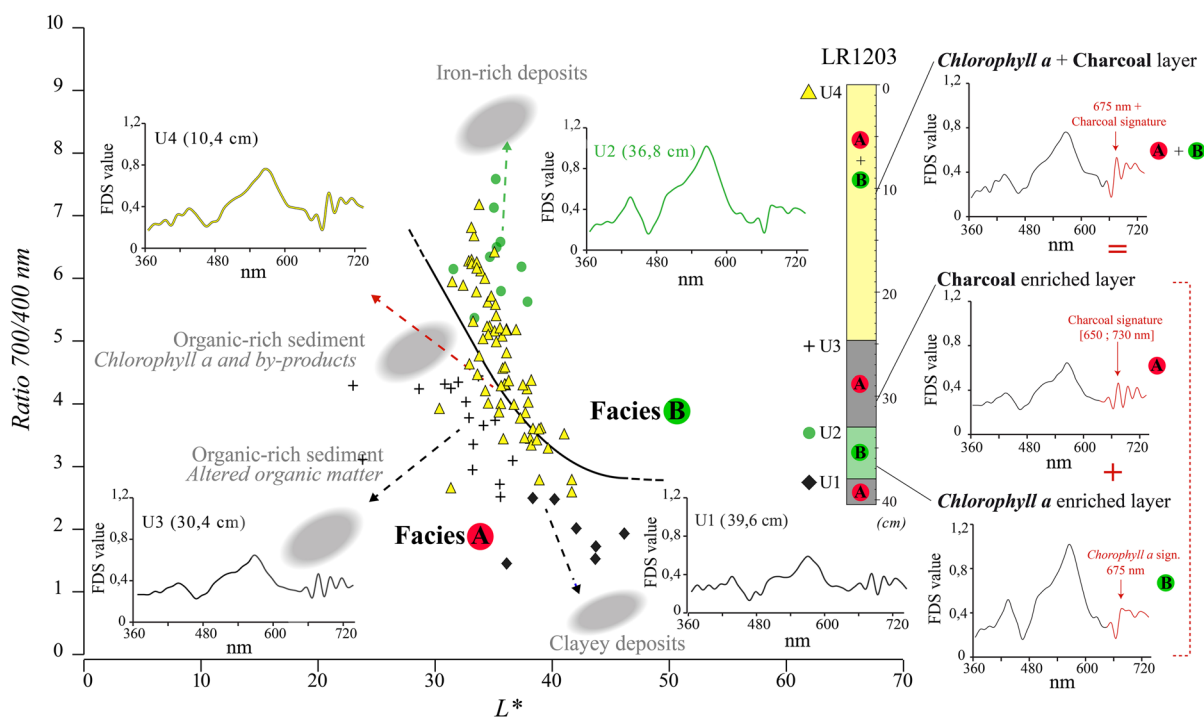


**Fig. 4** Q7/4 diagram showing sediment end-members. Sedimentary units are identified based on the first derivative spectra (FDS) signature of OM between wavelengths of 600 and 700 nm. Reference FDS signatures and examples for each unit

are presented. U1 and U3 have facies type B; U2 and U4 have facies type A. The additive property of first derivative signatures for the OM matter sources in U4 are illustrated on the right

the  $L^*$  values (mean of 20%) are the lowest of the studied sediment archive (Fig. 4). Throughout this unit, the signal of altered OM is identified, which agrees with the high concentrations of counted charcoal. The two points exhibiting the lowest  $L^*$  values in the Q7/4 diagram correspond to the dark lamina that marks a clear separation from the unit below (Fig. 4). This lamina reveals a clear signal of altered OM and corresponds to the highest concentration of charcoal. The constant values in the Chlorophyll *a* profile show the absence of a relationship between charcoal input and the Chlorophyll *a* concentration. U3 differs from the units above and below by the significant content of altered/carbonized (cf. charcoal) OM. Charcoal content decreases toward the top of U3.

U4 exhibits intermediate values for the Q7/4 ratio and  $L^*$  (Fig. 4). The samples from this unit encompass all the colorimetric characteristics of the previous units. The sediment here is marked by some mineral and organic inputs from the catchment as well as substantial organic primary productivity (peak at 675 nm with the altered OM signal), confirmed by macrocharcoal counting and Chlorophyll *a* concentrations. Some samples, however, tend towards the end-member diagnostic for altered OM and correspond to the black lamina in which the concentration of charcoal is high, indicating a brief input of carbonized OM from the catchment. Some depths in this unit lie outside of the general pattern of U4 and are located towards altered OM. This depth at 33 cm corresponds to the black layer, where the number of macrocharcoals reaches high values. The sharpness of this lamina seems to imply rapid input from the watershed.

## Discussion

### Organic matter sources

Although the carbonized OM (facies A; Fig. 4) and Chlorophyll *a* and its by-products (facies B; Fig. 4) have been identified by the FDS pattern at 675 nm, neither the Q7/4 ratio nor the FDS can track changes in OM sources throughout the core. This is because these two variables are influenced by the colour of the sediment matrix. To avoid this problem, we used the I-band index of Rein and Sirocko (2002) presented in Fig. 5. This method is based on the depth of the reflectance signal from 590 to 730 nm and normalised

by the average reflectance ( $R_{\text{mean}}$ ) to limit the sediment matrix effects (Rein and Sirocko 2002). Spectroscopic indexes used to track primary productivity are calculated and then calibrated against the concentration of Chlorophyll *a* and its by-products determined by HPLC (Wolfe et al. 2006). Applied to lacustrine sediment from the Arctic environment, these authors found that the area related to the signal depression around 670 nm, is proportional to the concentration of Chlorophyll *a* and its by-products. The Arctic environment was suitable for this calibration because the lake catchments were devoid of soil OM, geologic OM and residual OM from combustion.

In our study, we examined whether this method could be applied in an environment containing different OM sources, especially when the Chlorophyll *a* and its by-products are diluted by carbonized OM. Hence, we applied the I-band index to the spectrophotometric data and then to data obtained from the hyperspectral core scanner. The comparison between the sieving method (counting of charcoal particles) and the I-band index, applied to the spectrophotometric signals, clearly highlights several inputs of carbonized OM to the lake. Figure 5 compares, qualitatively, the two methods. As an example, at 32.5-cm depth, where the highest charcoal concentration was found (Fig. 5, point a), the spectrophotometric derivative signature of altered OM is well expressed (Fig. 5a). This correlation is even more striking between the macrocharcoal concentrations and hyperspectral data. For this purpose, the hyperspectral data (64- $\mu\text{m}$  resolution) were averaged to the sampling interval of the sieving method (Fig. 5c).

### Towards a new high-resolution fire proxy

To verify the efficacy of this new fire proxy in the sediments of Lake Bresson, the fire time series was compared with the fire events identified at high resolution in the core, dated by short-lived radionuclides. With respect to a threshold of charcoal particles of 150 counts, the charcoal concentrations, spectrophotometric and hyperspectral data display evidence for the occurrence of three major inputs of combustion residues, at depths of 38.0, 32.5 and 0.5 cm in the sediment.

The oldest event identified in the soil (U1) occurred before the dam was built, and it is therefore assumed that the charcoals stored in this ancient soil (before

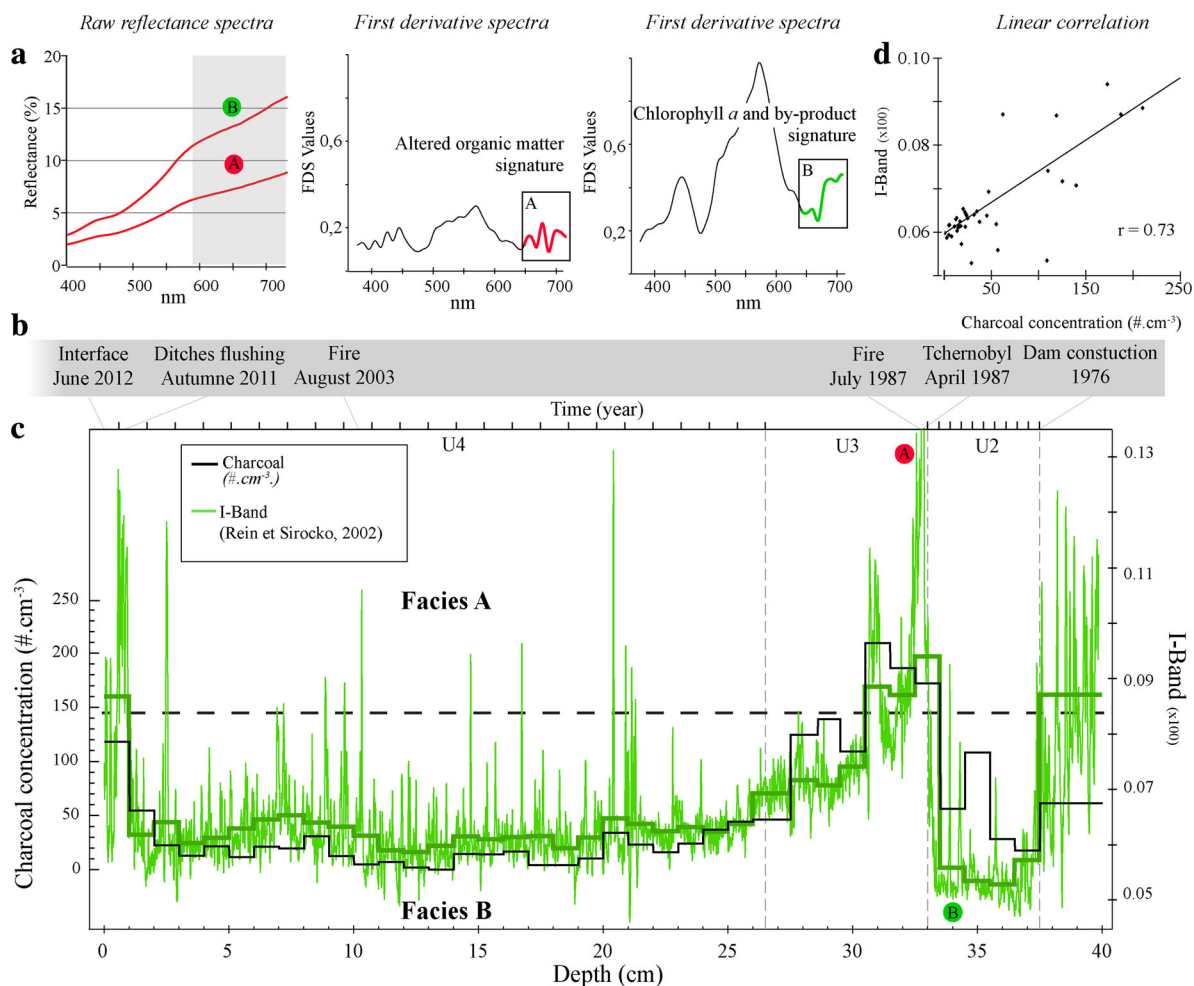


**Fig. 5** Fire event identification in hyperspectral data compared to charcoal concentration. **a** Spectra and FDS of sediments rich in altered OM and Chlorophyll *a*. **b** Chronological markers for core LR1203. **c** Comparison of charcoal concentration and

hyperspectral analyses (I-band) calculated according to Rein and Sirocko (2002). Hyperspectral data are averaged to the sampling interval of the sieving method. **d** Linear correlation between charcoal concentration and averaged I-band index

dam building) might be related to a wildfire that occurred in 1969 (fire records government service: Promethee data base at [www.promethee.fr](http://www.promethee.fr)). The wildfire that occurred in 1987 was responsible for the concentration of charcoal at the depth of 32.5 cm (extent of past fires that occurred after the lake formation are illustrated in Fig. 1). This event affected proximal parts of the catchment, but did not have an impact across the entire catchment (Fig. 1b).

The final event that supplied carbonized OM at 0.5 cm depth is dated to 2011, but no wildfire that affected the catchment or its vicinity was recorded in that year. According to the National Forestry Office, however, ditches alongside the paths that cross the

catchment (Fig. 1) were maintained during that year. This caused the remobilization of charcoal particles, accompanied by plant macrorests, which were subsequently deposited in the lake. Anthropogenic activities that lead to charcoal reworking, e.g. through soil erosion, could lead to false interpretations by producing artificial fire signals (Vanni re et al. 2003).

In 2003, a forest fire occurred in the catchment. Surprisingly, the spectrophotometric and hyperspectral data did not detect it. This inability to detect is not related to the method applied, since macrocharcoal counting also failed to identify the fire. Thus, the absence of a fire signal must be attributed to another cause, like wind direction during the fire event.

Indeed, this fire event only affected the northwestern part of the catchment (Fig. 1b) and as previously addressed by several studies (Clark 1988; Lynch et al. 2004; Higuera et al. 2007), the sediment record of the fire signal strongly depends on the proximity of the fire area. Another possible explanation for the absence of a sediment signal for the fire event in 2003 is the temporary storage of the charcoal in slope deposits within the catchment. These deposits could be eroded during intense rainfall (typical of the Mediterranean climate), which would release some charcoal in the ephemeral streams during runoff events. This could explain why there is permanent background loading of charcoal in the lake, observed both in the macrocharcoal counting and in the hyperspectral fire signals.

The Chlorophyll *a* concentrations did not allow identification of the fire signal. Indeed, we could expect to measure a low Chlorophyll *a* content immediately after the fire as a consequence of greater runoff caused by vegetation and soil destruction. That, however, is not the case. The Chlorophyll *a* concentration is constant over the fire event, indicating that the primary productivity remained unaffected by watershed disturbance. These results highlight the fact that the spectral index I-band cannot be used as a simple proxy for Chlorophyll *a* in environments dominated by terrigenous input. The interaction of charcoal with the Chlorophyll *a* signature, however, enables detection of the fire signal in sediment cores (Fig. 5).

## Conclusions

VIS-NIRS spectral measurements are non-destructive, rapid and do not require pre-treatment before analysis. Therefore, these methods have considerable advantages compared with the traditional methods used for OM characterization. By adapting the I-band index to hyperspectral data, the relative variations in charcoal concentration in lacustrine sediments were detected at very high resolution. With a spectral resolution of 6 nm in the range 400–1000 nm, and a spatial resolution of 64 × 64 μm, hyperspectral imaging is a promising method for inferring fire history at high resolution. In the foreseeable future, this method will be tested in catchments that contain different OM sources, such as geologic OM, in some cases possessing physical and chemical properties similar to

charcoal (i.e. from coalbeds), which can be released from sedimentary rocks by erosion and weathering processes.

**Acknowledgements** This work was funded by the Region Normandie, which supports the scientific consortium SCALE UMR CNRS 3730. Charcoal tallying was done at the UMR Chrono-environnement, Besançon, in the framework of Région Franche-Comté Project No. 2016YC-04552. We thank M. Fournier, University of Rouen for support, the Laboratoire Souterrain de Modane for the very-low-background radioactivity facilities, Emmanuel Viard for processing samples for HPLC analysis. A. Van Exem was responsible for data acquisition in Rouen, C. Butz in Bern. We are grateful to the two anonymous reviewers.

## References

- Appleby PG, Oldfield F (1992) Application of <sup>210</sup>Pb to sedimentation studies. In: Ivanovich M, Harmon RS (eds) Uranium series disequilibrium. Clarendon Press, Oxford, pp 731–778
- Appleby PG, Richardson N, Nolan PJ (1991) <sup>241</sup>Am dating of lake sediment. *Hydrobiologia* 214:35–42
- Balsam WL, Beeson JP (2003) Sea-floor sediment distribution in the Gulf of Mexico. *Deep Sea Res* 50:1421–1444. <https://doi.org/10.1016/j.dsr.2003.06.001>
- Balsam WL, Deaton BC (1996) Determining the composition of late quaternary marine sediments from NUV, VIS, and NIR diffuse reflectance spectra. *Marine Geol* 134:31–55
- Balsam WL, Damuth JE, Schneider RR (1997) Comparison of shipboard vs. shorebased spectral data from Amazon Fan cores: implications for interpreting sediment composition. *Ocean Drill Prog Sci* 155s:193–215
- Balsam WL, Deaton BC, Damuth JE (1999) Evaluating optical lightness as a proxy for carbonate content in marine sediment cores. *Marine Geol* 161:141–153
- Barranco FT, Balsam WL, Deaton BC (1989) Quantitative reassessment of brick red lutites—evidence from reflectance spectrophotometry. *Marine Geol* 89:299–314
- Butz C, Grosjean M, Poraj-Górska A, Enters D, Tylmann W (2016) Sedimentary Bacteriopheophytin a as an indicator of meromixis in varved lake sediments of Lake Jacznó, north-east Poland, CE 1891–2010. *Glob Planet Chang* 144:109–118
- Chatry C, Le Gallou Y, Le Quebrec M, Lafite J-J, Laurens D, Creuchet B, Grellu J (2010) Changement climatique et extension des zones sensibles aux feux de forêts. Rapport de la mission interministérielle
- Clark RN (1983) Spectral properties of mixtures of montmorillonite and dark carbon grains: implications for remote sensing minerals containing chemically and physically adsorbed water. *J Geophys Res* 88(10,635):10,644
- Clark JS (1988) Stratigraphic charcoal analysis on petrographic thin sections: application to fire history in northwestern Minnesota. *Quat Res* 30:81–91
- Dearing JA, Hu Y, Doody P, James PA, Rauer A (2001) Preliminary reconstruction of sediment-source linkages for the

- past 6000 years at the Petit Lac d'Annecy, France, based on mineral magnetic data. *J Paleolimnol* 25:245–258
- Deaton BC, Balsam WL (1991) Visible spectroscopy—a rapid method for determining hematite and goethite concentration in geological materials. *J Sediment Res* 61:628–632
- Debret M, Desmet M, Balsam W, Copard Y, Francus P, Laj C (2006) Spectrophotometer analysis of Holocene sediments from an anoxic fjord: Saanich Inlet, British Columbia, Canada. *Marine Geol* 229:15–28
- Debret M, Sebag D, Desmet M, Balsam W, Copard Y, Mourier B, Winiarski T (2011) Spectrocolorimetric interpretation of sedimentary dynamics: the new “Q7/4 diagram”. *Earth Sci Rev* 109:1–19. <https://doi.org/10.1016/j.earscirev.2011.07.002>
- Debret M, Bentele I, Sebag D, Favier C, Nguetsop V, Fontugne M, Oslisly R, Ngomanda A (2014) Influence of inherited paleotopography and water level rise on the sedimentary infill of Lake Ossa (S Cameroon) inferred by continuous color and bulk organic matter analyses. *Palaeogeogr Palaeoclimatol Palaeoecol* 411:110–121
- Goldberg E (1963) Geochronology with lead-210 radioactive dating. International Atomic Energy Agency, Vienna, pp 121–131
- Guilliano M, Mille G, Kister J, Muller JF (1988) Étude des spectres IRTF de charbons français déminéralisés et de leurs macéraux. *J Chim Phys* 85:963–970
- Higuera PE, Peters ME, Brubaker LB, Gavin DG (2007) Understanding the origin and analysis of sediment-charcoal records with a simulation model. *Quat Sci Rev* 26:1790–1809
- IPCC (2013) Climate change 2013: the physical science basis. IPCC Working Group I Contribution to AR5
- Krishnaswamy S, Lal D, Martin JM, Meybeck M (1971) Geochronology of lake sediments. *Earth Planet Sci Lett* 11:407–414
- Lafargue E, Marquis F, Pillot D (1998) Rock-Eval 6 applications in hydrocarbon exploration, production, and soil contamination studies. *Oil Gas Sci Technol* 53:421–437
- Lynch JA, Clark JS, Stocks BJ (2004) Charcoal production, dispersal, and deposition from the Fort Providence experimental fire: interpreting fire regimes from charcoal records in boreal forests. *Can J For Res* 34:1642–1656
- Milliken RE, Mustard JF (2007) Estimating the water content of hydrated minerals using reflectance spectroscopy: I. Effects of darkening agents and low-albedo materials. *Icarus* 189:550–573. <https://doi.org/10.1016/j.icarus.2007.02.017>
- Pausas JG (2004) Changes in fire and climate in the eastern Iberian Peninsula (Mediterranean basin). *Clim Change* 63:337–350
- Rein B, Sirocko F (2002) In-situ reflectance spectroscopy—analysing techniques for high-resolution pigment logging in sediment cores. *Int J Earth Sci* 91:950–954
- Reyss JL, Schmidt S, Legeleux F, Bonte P (1995) Large low background well type detectors for measurements of environmental radioactivity. *Nucl Instrum Methods* 357:391–397
- San-Miguel-Ayanz J, Pereira JMC, Boca R, Strobl P, Kucera J, Pekkarinen A (2009) Forest fires in the European Mediterranean region: mapping and analysis of burned areas. In: Chuvieco E (ed) *Earth observation of wildland fires in Mediterranean ecosystems*. Springer, New York, pp 189–203
- Schalles JF, Gitelson AA, Yacobi YZ, Kroenke AE (1998) Estimation of chlorophyll a from time series measurements of high spectral resolution reflectance in an eutrophic lake. *J Phycol* 34:383–390
- Sobkowiak M, Reisser E, Given P, Painter PC (1984) Determination of aromatic and aliphatic CH groups in coal by FTIR. 1. Studies of coal extracts. *Fuel* 63:1245–1252
- Thevenon F, Bard E, Williamson D, Beaufort L (2004) A biomass burning record from the West Equatorial Pacific over the last 360 ky: methodological, climatic and anthropic implications. *Palaeogeogr Palaeoclimatol Palaeoecol* 213:83–99
- Trachsel M, Kvisvik BC, Nielsen PR, Bakke J, Nesje A (2013) Inferring organic content of sediments by scanning reflectance spectroscopy (380–730 nm): applying a novel methodology in a case study from proglacial lakes in Norway. *J Paleolimnol* 50:583–592. <https://doi.org/10.1007/s10933-013-9739-1>
- Turner R, Kelly A, Roberts N (2008) A critical assessment and experimental comparison of microscopic charcoal extraction methods. In: Fiorentino G, Magri D (eds) *Charcoals from the past: cultural and palaeoenvironmental implications*. Proceedings of the third international meeting of anthracology, Cavallino (Lecce), June 2004. BAR international series. Archaeopress, Oxford, pp 265–272
- Vannièrè B, Bossuet G, Walter-Simonnet A-V, Gauthier E, Barral P, Petit C, Buatier M, Daubigney A (2003) Land use change, soil erosion and alluvial dynamic in the lower Doubs Valley over the 1st millennium AD (Neublans, Jura, France). *J Archaeol Sci* 30:1283–1299
- Vannièrè B, Colombaroli D, Chapron E, Leroux A, Tinner W, Magny M (2008) Climate versus human-driven fire regimes in Mediterranean landscapes: the Holocene record of Lago dell'Accesa (Tuscany, Italy). *Quat Sci Rev* 27:1181–1196
- Vannièrè B, Power MJ, Roberts N, Tinner W, Carrión J, Magny M, Bartlein P, Colombaroli D, Danialu AL, Finsinger W, Gil-Romera G, Kaltenrieder P, Pini R, Sadori L, Turner R, Valsecchi V, Vescovi E (2011) Circum-Mediterranean fire activity and climate changes during the mid Holocene environmental transition (8500–2500 cal yr BP). *Holocene* 21:53–73
- Whitlock C, Millsap SH (1996) Testing the assumptions of fire history studies: an examination of modern charcoal accumulation in Yellowstone National Park, USA. *Holocene* 6:7–15
- Wolfe AP, Vinebrooke RD, Michelutti N, Rivard B, Das B (2006) Experimental calibration of lake-sediment spectral reflectance to Chlorophyll a concentrations: methodology and paleolimnological validation. *J Paleolimnol* 36:91–100